

**AUTOMATIC DETECTION OF MELANOMA BASED  
ON THE ABCDE CRITERIA**

**PATRACHAI SACHATHAMAKUL**

**A SENIOR PROJECT SUBMITTED IN  
PARTIAL FULFILMENT  
OF THE REQUIREMENTS FOR  
THE DEGREE OF BACHELOR OF SCIENCE  
(COMPUTER SCIENCE)  
MAHIDOL UNIVERSITY INTERNATIONAL COLLEGE  
MAHIDOL UNIVERSITY  
2015**

**COPYRIGHT OF MAHIDOL UNIVERSITY**

Senior Project

entitled

**AUTOMATIC DETECTION OF MELANOMA BASED ON THE  
ABCDE CRITERIA**

was submitted to the Mahidol University International College, Mahidol University  
for the degree of Bachelor of Science (Computer Science)

on

3rd December 2015

.....  
Patrachai Sachathamakul  
Candidate

.....  
Piti Ongmongkolkul, Ph.D.  
Advisor

.....  
Aram Tangboondouangjit, Ph.D.  
Chair of Science Division  
Mahidol University International College  
Mahidol University

.....  
Kanat Tangwongsan, Ph.D.  
Program Director  
Bachelor of Science in Computer Science  
Mahidol University International College  
Mahidol University

## **ACKNOWLEDGEMENTS**

Firstly, I would like express my sincere gratitude to my senior project advisor Dr. Piti Ongmongkolkul for the continuous support, patience, motivation and immense knowledge. I would also like to give gratitude towards the related projects and papers involved in skin cancer detection algorithms. Moreover, the mature tools and libraries available for public use helped me a lot. I would also like to pay gratitude to all my lecturers who have shared their wisdom with me and gave me courage for four years. Last but not least, I am grateful for my friends and family's continuous support throughout my Bachelors degree.

Patrachai Sachathamakul

AUTOMATIC DETECTION OF MELANOMA BASED ON THE ABCDE CRITERIA.

PATRACHAI SACHATHAMAKUL 5480173 ICCS/B

B.Sc. (COMPUTER SCIENCE)

SENIOR PROJECT ADVISORS : PITI ONGMONGKOLKUL, PH.D., (COMPUTER SCIENCE)

ABSTRACT

This paper proposes a way to automatically detect Melanoma based on the ABCDE criteria. Melanoma is the most deadly form of skin cancer and it's steadily increasing. A popular technique for self-diagnosis of melanoma is to use the ABCDE criteria: asymmetry, border irregularity, color, diameter and evolution. This paper first examines two image segmentation algorithms where the goal is to separate the lesion from the background. Next, we utilize a couple of preprocessing techniques in order to prepare our image for feature extraction. Then, five features are extracted from the lesion in accord with the ABCDE criteria. Lastly, based on the features extracted, three versions of a support vector machines are studied to see the most suitable algorithm for melanoma detection: Linear SVM, Radial SVM and Quadratic SVM. We then study the experimental results and performance metrics for each step individually.

KEY WORDS : IMAGE PROCESSING / MACHINE LEARNING

58 pages

# CONTENTS

<b>ACKNOWLEDGEMENTS</b>	<b>iii</b>
<b>ABSTRACT (ENGLISH)</b>	<b>iv</b>
<b>LIST OF TABLES</b>	<b>vii</b>
<b>LIST OF FIGURES</b>	<b>viii</b>
<b>1 Background</b>	<b>1</b>
1.1 Human Skin . . . . .	1
1.2 Risk Factors of Melanoma . . . . .	2
1.3 ABCDEs of Melanoma . . . . .	4
<b>2 Introduction</b>	<b>9</b>
2.1 Problem Statement . . . . .	9
2.2 Project Scope . . . . .	10
2.2.1 Project Objectives/Motivation . . . . .	10
2.2.2 Possible Applications . . . . .	10
<b>3 Literature Review</b>	<b>12</b>
3.1 SkinVision . . . . .	12
3.2 IBM Skin Cancer Detection System . . . . .	13
<b>4 Implementation</b>	<b>14</b>
4.1 Tools used . . . . .	14
4.1.1 NumPy and Pandas . . . . .	14
4.1.2 SciKit . . . . .	15
4.2 Data Collection . . . . .	15
4.3 Image Preprocessing . . . . .	16
4.3.1 RGB to Grayscale . . . . .	17
4.3.2 Normalizing the Size . . . . .	17
4.3.3 Noise Reduction . . . . .	17
4.4 Image Segmentation . . . . .	19
4.4.1 Otsu's Method (Thresholding) . . . . .	19
4.4.2 Morphological Active Contour Without Edges (MACWE) . . . . .	23
4.5 Feature Extraction . . . . .	24
4.5.1 Asymmetry . . . . .	25

## CONTENTS (CONT.)

vi

4.5.2	Border Irregularity . . . . .	27
4.5.3	Color . . . . .	30
4.5.4	Diameter . . . . .	35
4.5.5	Evolution . . . . .	37
4.6	Classification Model . . . . .	37
4.6.1	Linear SVM . . . . .	39
4.6.2	Radial Kernel . . . . .	40
4.6.3	Quadratic Kernel . . . . .	40
<b>5</b>	<b>Experimental Results</b>	<b>42</b>
5.1	Preprocessing Results . . . . .	42
5.2	Image Segmentation Results . . . . .	42
5.3	Statistical Summary of Feature Extraction . . . . .	44
5.4	Scatterplot Summary of Feature Extraction . . . . .	46
5.5	Classification Results . . . . .	48
<b>6</b>	<b>Conclusion</b>	<b>54</b>
6.1	Future Work . . . . .	54
<b>REFERENCES</b>		<b>55</b>
<b>BIOGRAPHY</b>		<b>58</b>

## LIST OF TABLES

1.1	Survival rates of different stages of Melanoma . . . . .	5
5.1	Impact of preprocessing images . . . . .	42
5.2	Comparison of MACWE and Otsus Method . . . . .	43
5.3	Statistics of features extracted . . . . .	45
5.4	Comparison of algorithms' accuracy rates at default threshold of 0.5 . . . . .	49
5.5	Confusion matrix for Suppor Vector Machine (Linear) . . . . .	50
5.6	Confusion matrix for Suppor Vector Machine (Radial) . . . . .	50
5.7	Confusion matrix for Suppor Vector Machine (Quadratic) . . . . .	50
5.8	ROC Analysis Summary at threshold = 0.5 . . . . .	51

## LIST OF FIGURES

1.1	Human Skin Anatomy . . . . .	2
1.2	Where Melanoma is most likely to develop . . . . .	3
1.3	Lifetime risk of getting melanoma by country and gender . . . . .	4
1.4	Comparison of asymmetry between melanoma and a benign mole . . . . .	5
1.5	Comparison of border irregularity between melanoma and a benign mole . . . . .	6
1.6	Example of a malignant moles different colors . . . . .	7
1.7	Example of a measuring a malignant moles diameter with a measuring tape . . . . .	7
1.8	Example of a malignant moles evolution over time . . . . .	8
3.1	SkinVision Mobile Application . . . . .	12
4.1	Implementation Flowchart . . . . .	14
4.2	Example of images where there is light reflection (left), the image is blur (middle) and where there is image noise which in this case is body hair (right) . . . . .	16
4.3	Example Result of Median Filtering . . . . .	18
4.4	Median Filtering . . . . .	19
4.5	Comparison of a well segmented lesion (left) with a poorly segmented lesion (right) . . . . .	20
4.6	Image segmentation using different thresholds . . . . .	21
4.7	Example of histogram plot from a greyscale image . . . . .	22
4.8	Possible cases of the position of the curve . . . . .	24
4.9	Simulation of MACWE algorithm . . . . .	25
4.10	Example centroid location . . . . .	26
4.11	Examples of asymmetry index . . . . .	27
4.12	Example of an image of low edge abruptness . . . . .	28
4.13	Example of an image of high edge abruptness . . . . .	28
4.14	Examples of edge abruptness equation . . . . .	30
4.15	Example of clustering . . . . .	31
4.16	Image with high lighting conditions . . . . .	32
4.17	Color extraction phase of Figure 4.16 . . . . .	33
4.18	Two examples of color variation for red value . . . . .	34
4.19	Two examples of relative chromaticity for red value . . . . .	36

## LIST OF FIGURES (CONT.)

ix

4.20	Image with high zoom . . . . .	36
4.21	Image with low zoom . . . . .	37
4.22	Support Vector Machine . . . . .	39
4.23	RBF Kernel Trick . . . . .	41
5.1	Comparison of a well segmented lesion (left) with a poorly segmented lesion (right) . . . . .	43
5.2	How MACWE and Otsu's Method deals with large noise . . . . .	44
5.3	Scatterplot summary of feature extraction (part 1) . . . . .	47
5.4	Scatterplot summary of feature extraction (part 2) . . . . .	48
5.5	Comparison of algorithms using ROC Curve . . . . .	53

# CHAPTER 1

## BACKGROUND

Before we discuss this paper's research, we must explore the nature of the cancer. This chapter explores the human skin, risk factors, stages and ABCDEs of melanoma. If you would like to skip this chapter, please go to Chapter 2.

Melanoma accounts for four percent of all skin cancers, however it is the deadliest, responsible for approximately 80% of all skin-cancer related deaths. According to the National Cancer Institute (USA), 73,870 new melanoma cases in the USA are predicted to be diagnosed in 2015 where 9,940 (approximately 13.4%) of them are expected to die from melanoma [32].

### 1.1 Human Skin

Human skin is separated into three layers: the epidermis, the dermis and the subcutis (as illustrated below).

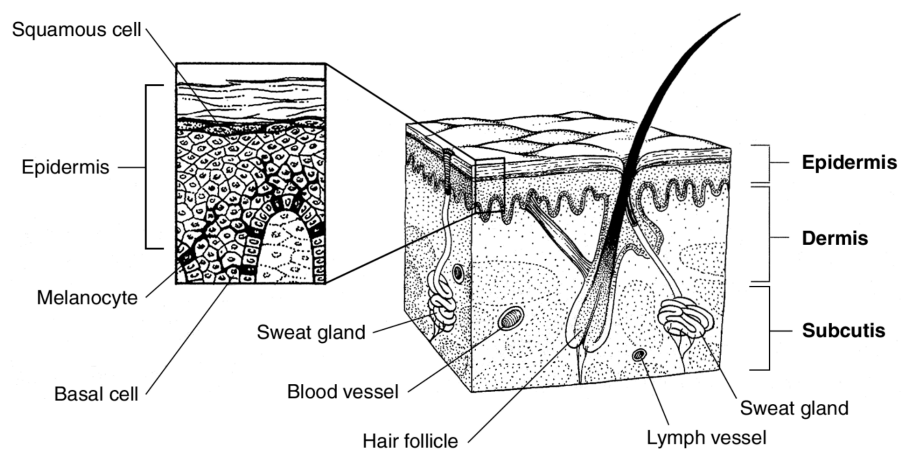


Figure 1.1: Human Skin Anatomy

**Epidermis:** This is outer-most layer of skin which is very thin, averaging to only about 1/100 of an inch thick. The main cells of the epidermis include:

- Squamos cells: Thin, flat cells in the outer layer of the epidermis which are constantly shedding and reformed
- Basal cells: These cells constantly divide to replace squamos cells
- Melanocytes: These cells make a brown pigment called melanin, which gives the skin its tan or brown color. Melanin protects the inner layers of the skin from sun rays. For the majority of the people, when the skin is exposed to the sun, melanocytes produce more melanin, causing the skin to tan. Melanocytes are the cells that can become melanoma.

Dermis: This is the middle layer of the skin which is much thicker than the epidermis. This layer is mainly composed of hair follicles, sweat glands, blood vessels and lymph vessels.

Subcutis: This is the deepest layer of the skin and the lowest part of the dermis which is formed of collagen and fat cells. The subcutis is responsible for conserving body heat and to protect the inner organs. [32]

## 1.2 Risk Factors of Melanoma

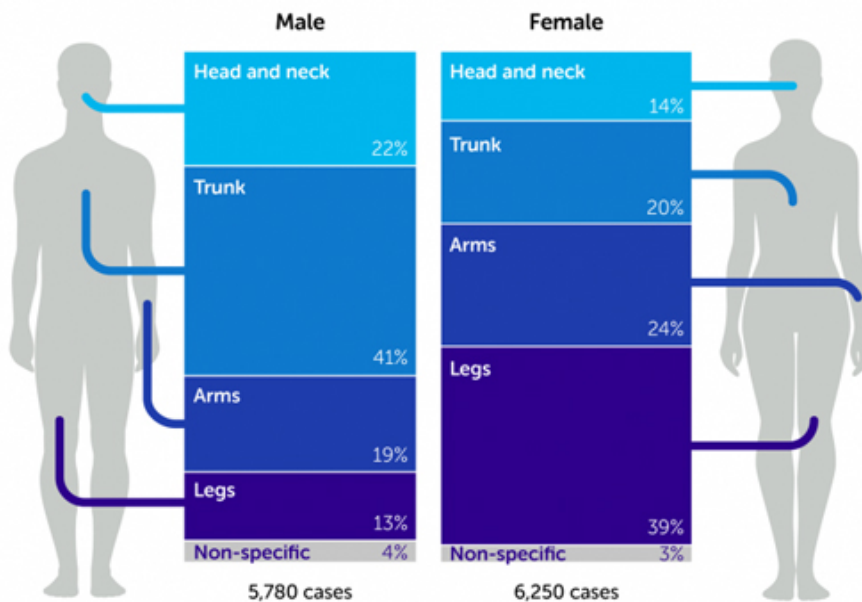


Figure 1.2: Where Melanoma is most likely to develop

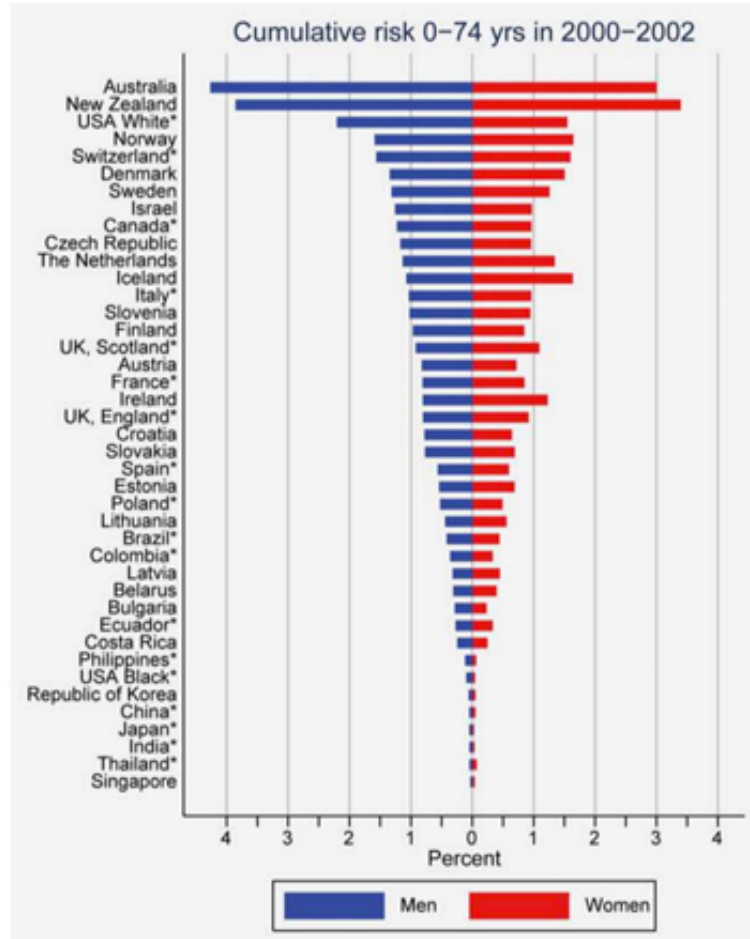


Figure 1.3: Lifetime risk of getting melanoma by country and gender

Melanoma is a cancer that begins from melanocytes, located in the epidermis of human skin. As demonstrated in Figure 1.2, we can see the distribution of places in the body where melanoma is likely to develop for Males (left) and Females (right), according to Melanoma cases in the UK from 2008 - 2010 [35].

Even though there are no conclusive reasons why melanoma occurs, below we discuss some popular risk factors involved:

1. Ultraviolet (UV) light exposure is a major risk factor for most melanoma cases. UV rays damage the DNA of the skin cells and skin cancer begins when the damaged cells affects the skin cells growth. Sunlight, tanning beds and sun lamps are some sources of UV rays.
2. Nevus, also known as a common mole, is a benign skin tumor that are developed

from melanocytes. Nearly all moles are harmless, however, they have a small chance to develop into melanoma.

3. The risk of Melanoma is much higher for whites or fair-skinned individuals. As illustrated in Figure 1.3, we can see that Melanoma is predominant among Caucasians and very rare for Asian and dark-skinned countries [8].
4. Family history and personal history also play a big factor. Around 10% of people diagnosed with melanoma have a family history of the disease. Moreover, about 5% of people with melanoma will develop a second one at some point in their lives. [32]

	<b>5-Year Survival Rate</b>	<b>10-Year Survival Rate</b>
<b>Stage 1A</b>	97%	95%
<b>Stage 1B</b>	92%	86%
<b>Stage 2A</b>	81%	67%
<b>Stage 2B</b>	70%	57%
<b>Stage 2C</b>	53%	40%
<b>Stage 3A</b>	78%	68%
<b>Stage 3B</b>	59%	43%
<b>Stage 3C</b>	40%	24%
<b>Stage 4</b>	15 to 20%	10 to 15%

Table 1.1: Survival rates of different stages of Melanoma

### 1.3 ABCDEs of Melanoma

The good news for people is that if Melanoma is diagnosed early, it could be treated and cured in most cases. As we can see from Table 1.1, if we can detect Melanoma early, it is almost always curable.

Developed by Alfred Kopf, Robert Friedman and Darrell Rigel in 1985, ABCDE is the most popular technique used to identify the signs and symptoms of Melanoma. This technique can be conducted by any individual and if one or more of the signs are

identified, an appointment with a dermatologist or a physician is urged. The ABCDE technique is as follows [6]:

A - Asymmetry



Figure 1.4: Comparison of asymmetry between melanoma and a benign mole

Benign moles are mostly symmetrical while malignant moles (melanoma) are asymmetrical. By splitting the mole vertically and horizontally, one can compare them (left to right, up to down) and analyze their symmetry. As illustrated in Figure 1.4, we can see that the benign mole is much more symmetric than the malignant mole.

B - Border Irregularity

Benign moles have smooth, even borders while malignant moles have abrupt, uneven borders. In Figure 1.5, we can see that the malignant mole (right) has irregular and uneven borders while the benign moles have more smoother, curved borders.



Figure 1.5: Comparison of border irregularity between melanoma and a benign mole

C - Color

Most benign moles have one shade of color (usually pink, brown or black), how-

ever, malignant moles have a variety of different colors. As shown in Figure 1.6, we can see that the malignant mole comprises of four main colors: dark shade of pink, light shade of pink, brown and very dark brown.



Figure 1.6: Example of a malignant moles different colors

D - Diameter The diameter of the mole is also an important factor when trying to figure out whether a mole is malignant or benign. Benign moles usually have small diameters while malignant moles usually have diameters greater than 0.25 inches. A simple way to measure the size of a mole is to use a measuring tape or a ruler.



Figure 1.7: Example of a measuring a malignant moles diameter with a measuring tape

#### E - Evolution

This is a very important feature which generally implies danger. If a mole



Figure 1.8: Example of a malignant moles evolution over time

changes/evolves in size, shape, color, elevation or any other trait, it is crucial to go visit a doctor.

## CHAPTER 2

### INTRODUCTION

#### 2.1 Problem Statement

As expressed above, Melanoma is a rare form of skin cancer, only accounting for four percent of all skin cancers, but is responsible for 80% of all skin cancer deaths [32]. Due to the stealthy and deadly nature of this cancer, Melanoma is a heavily researched topic and its preventive measures are becoming more and more sufficient. However, the number of Melanoma diagnoses have been steadily increasing for the past 50 years in most fair-skinned populations and is predicted to maintain the trend [8].

Government institutions and cancer foundations are actively trying to create awareness for Melanoma worldwide. For example, Melanoma Research Foundation (USA) regularly holds events such as Miles for Melanoma, Celebrity Golf Classic and GetNaked. For example, GetNaked is an event where people perform self-examinations and spread awareness through social media platforms [5]. Foundations like these also provide assistance and education for screening of Melanoma using the ABCDE checklist.

As mentioned in Section 1.3, the ABCDE checklist is a great technique for melanoma self-screening. If one or more of the signs of ABCDE are identified, people are urged to visit a physician or dermatologist immediately. This is a great way for people to recognize dangerous moles early and go to a medical professional. However, self-screening can be quite subjective. For example, the naked eye might find trouble trying to distinguish a symmetric mole from an asymmetric mole. Moreover, it might be hard to determine whether a mole has different shades of colors or not.

Lastly, we must also recognize the issue of misdiagnosis. Misdiagnosis is when a patient is wrongly diagnosed of a disease, or diagnosed the correct one too late. According to a research paper from BMJ Journal in 2014, approximately 12 million US outpatients

(adults) every year are misdiagnosed; 1 in 20 people [10]. For skin cancer in general, a study conducted by the American Society for Dermatological Surgery concluded that 90% of dermatological surgeons stated that they had at least one patient whom they have misdiagnosed [3].

## 2.2 Project Scope

As an attempt to solve the issues mentioned above, this paper proposes a way to help diagnose Melanoma while using the ABCDE symptom checker. Through thorough research, image processing techniques and machine learning algorithms, this research paper aims to correctly diagnose Melanoma.

### 2.2.1 Project Objectives/Motivation

- To better understand Melanoma and its features involved using the ABCDE criteria
- To gain knowledge in image processing techniques, including image segmentation, feature extraction and preprocessing. As I have no prior experience in image processing, this project gives me the opportunity to further my knowledge
- To implement a model which is used to predict whether a mole is benign or cancerous from images
- To evaluate my model and discuss the advantages/disadvantages of the model and how I can improve it

### 2.2.2 Possible Applications

If my research project deems successful, there are a variety of possible applications and extensions:

- Mobile application for users to diagnose and track their moles using images from their phones camera
- Software for hospitals and clinics where doctors can verify their diagnosis with the softwares prediction

- Expand the algorithm to detect and diagnose other types of skin conditions such as squamos-cell carcinoma and basal-cell carcinoma

## CHAPTER 3

### LITERATURE REVIEW

#### 3.1 SkinVision

SkinVision is a smartphone application which automatically analyses and detects early stages of Melanoma. The mobile app requires the user to take a photo of the suspected lesion and its algorithm will provide a risk rating. It is available on iOS devices (iPhone, iPad) and Android devices [30].

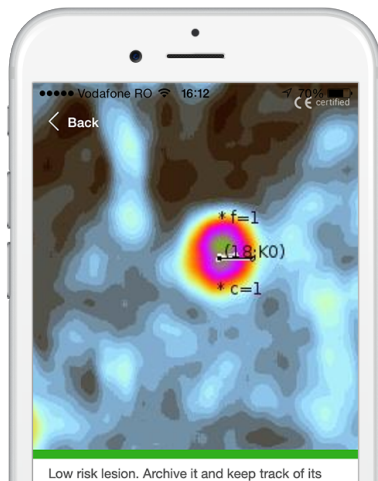


Figure 3.1: SkinVision Mobile Application

SkinVision is the first skin cancer mobile application to be CE marked. The CE mark is a product assessment which, if approved, claims that the product/service meets the essential requirements of European Medical Device Directives. This mark is a legal requirement to place a product/service on the market in the European Union (EU) [2].

Being one of the first mobile applications for skin cancer diagnosis, SkinVision has been featured in an array of medical journals and news blogs. In a study published in the Journal of the European Academy of Dermatology and Venereology in 2013, they found that SkinVision was 81% accurate in detecting Melanoma [31]. However, SkinVision

warns that this mobile app shouldnt replace medical professionals, but instead make people more aware of their skin.

There is one limitation to this mobile application - SkinVisions images are taken from phone cameras. Phone cameras are susceptible to causing a misdiagnosis due to several reasons such as image blurriness, image shakiness, inability to zoom in while maintaining quality and inconsistent lighting conditions.

### 3.2 IBM Skin Cancer Detection System

International Business Machines (IBM) is a multi-national technology and consulting corporation known for their numerous technological contributions. One of their major contributions to Artificial Intelligence is a supercomputer nicknamed Watson. Watson was built to mirror the same learning process that humans have; observe, interpret, evaluate and decide. Watson uses its scalable cognitive framework to gain and achieve expert level knowledge [37]. Through Watsons Developer Cloud, which is a library of APIs and SDKs, there are numerous applications in natural language processing, business analytics, healthcare and much more.

In December 2014, IBM Research announced a partnership with New Yorks Memorial Sloan Kettering Cancer Center to research the application of Watsons cognitive computing to analyze dermatological images with a goal of identifying various skin cancers. By using Memorial Sloan Ketterings 3,000 dataset of dermoscopic images, they were able to achieve an accuracy of approximately 95%. This is a staggering increase of accuracy rate as opposed to the previous diagnostic accuracy of 75 - 84% [38].

As of October 14, 2015, IBMs skin cancer detection system is still in the research phase where they have increased their dataset to around tens of thousands of melanoma images. They have also expanded their research centers to Victoria, Australia in October, 2015 [39].

## CHAPTER 4

### IMPLEMENTATION

Implementing a predictive model requires several processes which are illustrated in Figure 4.1. Through this chapter, we will explain these processes in detail.

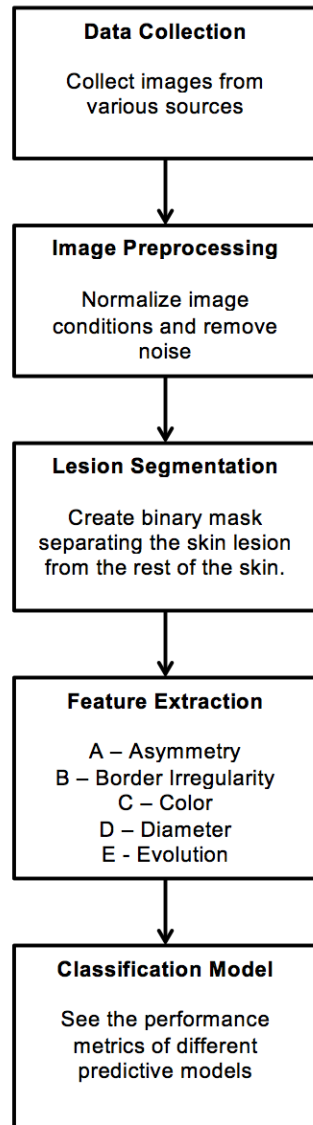


Figure 4.1: Implementation Flowchart

## 4.1 Tools used

Python is an open source general-purpose programming language which is commonly used for scientific scripting and data manipulation. Due to its large extension of libraries and tools, it was chosen as my primary programming language for this research project. The Python version used in this project is 2.7.8. The development environment we used was through IPython Notebook.

### 4.1.1 NumPy and Pandas

NumPy is a fundamental package used for scientific computing in Python. This package boasts many popular features such as n-dimensional array manipulations, broadcasting functions and high-level mathematical functions. NumPy has been used throughout my research project especially in instances where we needed to make statistical calculations (e.g. mean, standard deviations) and array-wise operations (e.g. array multiplication, inverting arrays).

Based on NumPys array-wise architecture, Pandas is a high-performance easy-to-use data structure and data analysis tool for Python. We used Pandas for my project in order to work with numerical and tabular data in an easier fashion.

### 4.1.2 SciKit

SciKit is a collection of algorithms developed by SciPy which is used for scientific and technical computing. It is subdivided into many several packages as follows:

- SciKit-Image is an image processing library which includes of algorithms for color space manipulation, geometric calculations, morphology and much more. SciKit-Image was used in my research project to calculate geometry properties of an image (perimeter and area) and to perform color conversions for images (RGB to greyscale).
- SciKit-Learn is a data mining and machine learning library including of an array of classification, regression, clustering algorithms and more. This package was

used in my research project to classify the melanoma images using support vector machines.

## 4.2 Data Collection

Reliable databases of Melanoma images are hard to acquire due to several reasons. Firstly, the images must be taken with a dermatoscope, which is a common instrument used by dermatologists to analyze skin lesions. Using a dermatoscope is proven to improve diagnostics by 15.6% as opposed to a naked eye diagnosis [36]. Secondly, the lighting conditions of the images must be standardized with all photos. Most importantly, the skin lesions must be determined by an expert whether they are malignant or benign.

The images which we're using for this research project is from a variety of sources. From the 109 images gathered, 74 of them are malignant and 35 benign. The sources of images are from reliable sources ranging from university websites, government websites and dermatology organizations. All of the image sources have license agreements which allows it to be used for a research project. The references to these sources can be found here: [11], [17], [18], [19], [20], [21], [22], [23], [24], [12], [13], [14], [15], [16].

## 4.3 Image Preprocessing

Due to the unstable and inconsistent conditions of the photos, preprocessing the image will play a huge impact on the image segmentation results. There are many visual distortions which may or may not appear in an image. Some of these are represented in Figure 4.2 below. In this section, we will explain the steps we took in order to preprocess images.

### 4.3.1 RGB to Grayscale

Most of the functions in the image segmentation and feature extraction phase require an image to be of greyscale. For this reason, the first thing we did was convert an RGB image to greyscale. An RGB image consists of red, green and blue values for each pixel



Figure 4.2: Example of images where there is light reflection (left), the image is blur (middle) and where there is image noise which in this case is body hair (right)

which range from an intensity of 0 to 255. Whereas a grayscale image pixels consist of a single intensity value from 0 to 255. The formula to convert an RGB image to a greyscale image is displayed below [7]:

$$Grey = 0.2125R + 0.7154G + 0.0721B \quad (4.1)$$

### 4.3.2 Normalizing the Size

Next, before segmenting and denoising the image, we must normalize the size of the image. Since size varies depending on images, we cannot treat them the same way and instead must normalize them. For this project, we normalized all images to have a base width of 340 pixels. Please note that the aspect ratio of the images are maintained.

### 4.3.3 Noise Reduction

Noise reduction, or also known as denoising, is considered a very important step in preprocessing. Images taken with digital cameras will pick up noise from a variety of sources. For example, as we can see in 4.3, body hair is a type of noise which must be taken care of. If we dont deal with the hair before-hand, our image segmentation algorithm will treat the hair as part of the skin lesion, and therefore will affect the feature extraction stage.

There are many algorithms which are used in order to denoise an image. We will discuss two popular algorithms used which are mean filtering and median filtering. Mean filtering is a simple, intuitive way for smoothing images by reducing the variation between one pixel and its neighboring pixels. The algorithm goes through each pixel in the image, and replace each pixel with the mean value of its neighboring pixels. Median

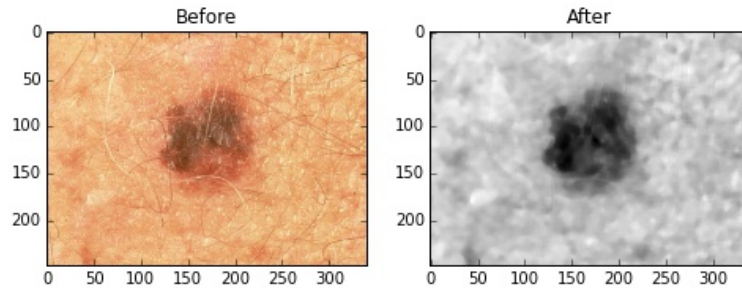


Figure 4.3: Example Result of Median Filtering

filtering is a very similar concept to mean filtering. The only difference is that, instead of replacing the current pixel with the neighbors mean pixel, it takes the median pixel instead. Both median and mean filtering don't change the shape of the image.

This could be viewed using the example in Figure 4.4. If we perform mean filtering for the blue pixel in the figure above, the pixel value will be:  $(3 + 5 + 2 + 4 + 4 + 7 + 5 + 6 + 5) / 9 = 4.56$ . If we perform median filtering for the blue pixel, the value will be 5 since the median value of 2, 3, 4, 4, 5, 5, 5, 6, 7 is 5.

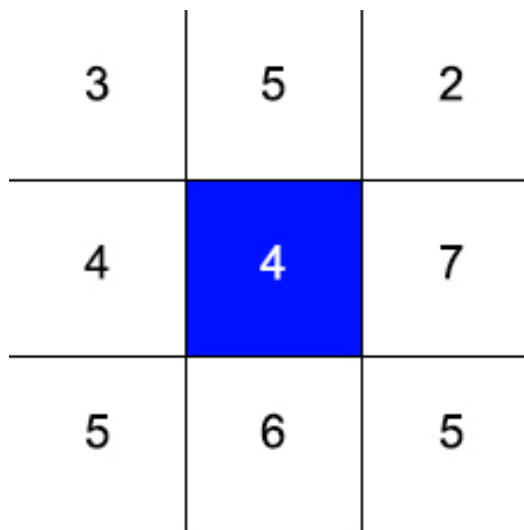


Figure 4.4: Median Filtering

In this project, we chose to use median filtering rather than mean filtering for a radius of 5 pixels. This is because mean filtering uses the image hair color as well as

the skin colors to estimate the color of a pixel. Since the number of hair pixels is usually smaller than the number of skin pixels in an image, when median filtering is used, the color of a pixel belonging to the hair will not be used since we only take the median value.

#### 4.4 Image Segmentation

The goal of image segmentation is to create a binary representation of an image separating the foreground with the background and is a common task in many image processing applications. Image segmentation is the forefront of this paper's melanoma detection algorithm. By correctly segmenting the lesion (benign or malignant) from the background, we can then proceed to correctly extract features, and finally to predict a diagnosis. In this project we compare the algorithms and results of two algorithms called Otsus method and morphological active contours without edges (MACWE). Firstly, Otsus method is a very popular technique used for basic image segmentation due to its implementation simplicity. It is featured in an array of medical imaging papers as identified in [27]. Secondly, inspired by P. Marquez Neilas paper [28], we chose to use their publicly accessible Python implementation of Morphological Active Contours Without Edges (MACWE).

The detail of the methods and algorithms can be found below.

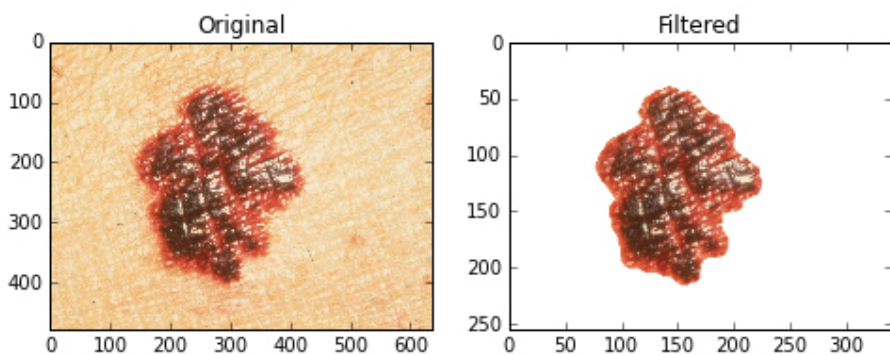


Figure 4.5: Comparison of a well segmented lesion (left) with a poorly segmented lesion (right)

#### 4.4.1 Otsu's Method (Thresholding)

Thresholding is a very common way to segment an image. Thresholding assumes that the image has two classes of pixels (foreground or background). By iterating through every pixel of the image, the algorithm calculates whether the pixels luminosity value is greater than the threshold (foreground) or less than the threshold (background).

Image segmentation using threshold is usually derived from the following steps:

1. Convert RGB image into grayscale (grayscale pixels will have an intensity value of 1 to 255)
2. Plot a histogram of pixels intensity values and its occurrences in the image
3. Choose a suitable threshold based on histogram

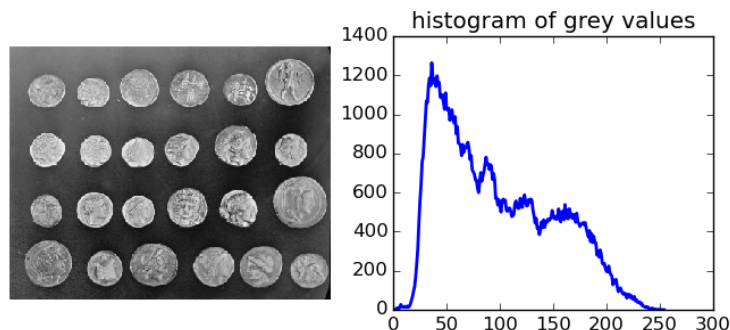


Figure 4.6: Image segmentation using different thresholds

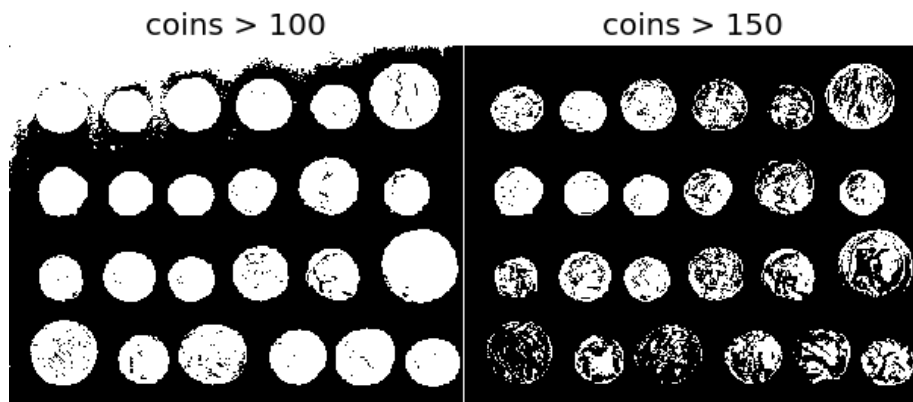


Figure 4.7: Example of histogram plot from a greyscale image

As demonstrated in Figure 4.7, we can see the impact of changing the threshold value from 100 and 150. This is the difficult part is picking a suitable threshold value for an image. Otsus method offers a solution for finding an optimal threshold. Otsus method suggests that the best threshold is the one which minimizes the intraclass variance of the threshold and therefore maximizing the interclass variance [9].

This following function calculates the intraclass variance:

$$\sigma_w^2(t) = q_1(t)\sigma_1^2(t) + q_2(t)\sigma_2^2(t) \quad (4.2)$$

Where:

- $t$  = threshold,
- $\sigma_1(t) = \sum_{i=1}^t P(i)$
- $\sigma_2(t) = \sum_{i=t+1}^I P(i)$
- $\mu_1(t) = \sum_{i=1}^T \frac{iP(i)}{q_1(t)}$
- $\mu_2(t) = \sum_{i=t+1}^I \frac{iP(i)}{q_2(t)}$
- $\sigma_1^2(t) = \sum_{i=1}^t [i - \mu_1(t)]^2 \frac{P(i)}{q_1(t)}$
- $\sigma_2^2(t) = \sum_{i=t+1}^I [i - \mu_2(t)]^2 \frac{P(i)}{q_2(t)}$

This means that  $P(i)$  is the probably of the intensity value of pixel  $i$  in the histogram,  $q_1$  is the sum of pixel intensity values from the 1 to the threshold,  $q_2$  is the sum of pixel values from the threshold to 255.  $u_1$  and  $u_2$  being the mean of class 1 and class 2.  $\sigma_1$  and  $\sigma_2$  is the variance for class 1 and class 2. Hence, after applying these values into the intraclass variance equation for every threshold from 1 to 255, we can take the lowest one to be the best threshold.

However, there are some notable limitations to Otsus threshold:

- Algorithm assumes that the histograms are bimodal

- Algorithm assumes that the illumination (0 to 255) is uniform

Due to these limitations, Otsus methods perform poorly with dermatological images (results will be discussed in 5). In the next section, we will discuss a more complex algorithm which could resolve the above limitations.

#### 4.4.2 Morphological Active Contour Without Edges (MACWE)

Active Contours (or a variation of) are commonly used in computer vision tools, specifically, edge and boundary detection. There have been many algorithms and techniques which are heavily researched with active contours and one of the outstanding one is Chan-Veses algorithm: Morphological Active Contour Without Edges (MACWE). MACWE defines an energy function for image segmentation which takes into account of the interior and exterior of a curve. This energy function is used to specify how the curve should evolve in order to minimize the energy.

The function of a curve C is defined by:

$$F(C, c_1, c_2) = \mu \cdot \text{length} + v \cdot \text{area}(insideC) + \lambda_1 F_1(C) + \lambda_2 F_2(C) \quad (4.3)$$

Where:

$$F_1(C) = \int_{inside(C)} |u_0 - c_1|^2 \quad (4.4)$$

$$F_2(C) = \int_{outside(C)} |u_0 - c_2|^2 \quad (4.5)$$

Where  $\mu$  (strength of smoothing),  $v$  (balloon force parameter),  $\lambda_1$  (importance of inside pixels) and  $\lambda_2$  (importance of outside pixels),  $c1$  (mean intensity values inside the curve  $u_0$ ) and  $c2$  (mean intensity values outside the curve  $u_0$ ) are non-negative parameters and I is image. The function F can be referred to as the cost function and our goal is to minimize it.

Most importantly,  $F_1$  gives us the variance of the color inside the curve while  $F_2$  gives us the variance outside of the curve. Our goal is to minimize both these variances. Let's describe this further using an example. Image  $u_0$  contains two piecewise-constant ( $u_0^i$  and  $u_0^o$ ). Moreover, let's assume that the object to be detected is  $u_0^i$ . Now let's

consider a perfect curve where  $u_0 u_i^0$  inside the object (inside C) and  $u_0 u_o^0$  outside the object [34]. In this case,  $F_1(C) + F_2(C) = 0$ . Other cases can be visualized below:

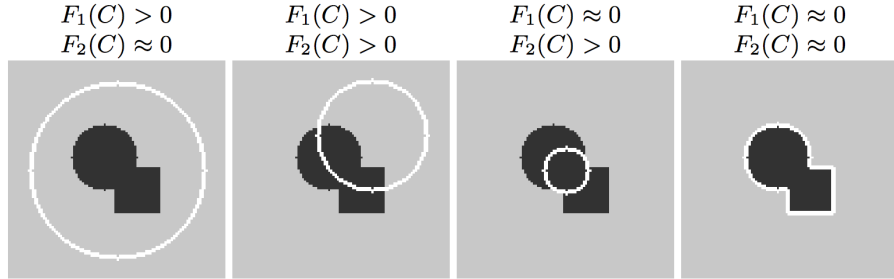


Figure 4.8: Possible cases of the position of the curve

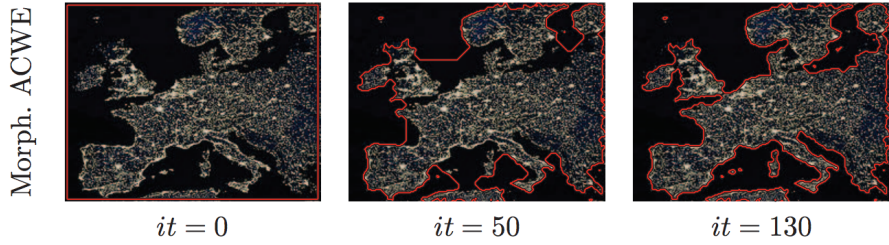


Figure 4.9: Simulation of MACWE algorithm

[28]

#### 4.5 Feature Extraction

In the broad spectrum of machine learning and pattern recognition, feature extraction is the process where measured data is derived from an input value intended to be informative to the learning stage. In our case, we are concerned about the visual features of an image, more specifically the ABCDEs. More information on the ACDEs of melanoma can be found in Section 1.3. This section demonstrates how we implemented feature extraction algorithms/equations in order for my research project to analyze skin images autonomously. Please note that we only perform feature extraction and evaluate the model with successfully segmented images.

#### 4.5.1 Asymmetry

The first feature which we must study is the asymmetric property of a skin lesion. Before we attempt to compare the symmetric/asymmetric values, we need to find the centroid of an image. A centroid is the center of a geometric object found by the arithmetic mean of all points in the shape. Its formula is defined as follows:

$$\text{centroid}_{\text{img}} = (\bar{x}, \bar{y}) = \left( \frac{\sum_{i=1}^N x_i}{N}, \frac{\sum_{i=1}^N y_i}{N} \right) \quad (4.6)$$

where  $\bar{x}$  and  $\bar{y}$  are the mean x and y pixels and N is the number of x and y pixels respectively.

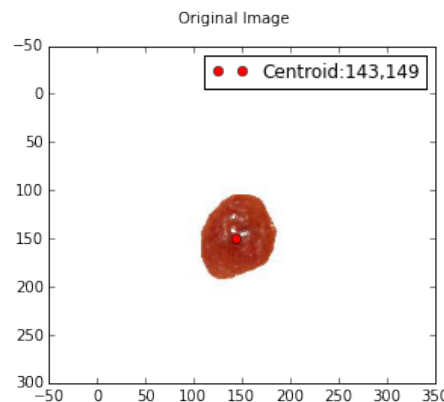


Figure 4.10: Example centroid location

Once we have determined the centroid of a lesion, we now need to split the image by its y-axis of symmetry and overlap the two sides in order to determine their disparity. We do the same with the x-axis of symmetry and compare the top half with the bottom half of the image to determine their disparity as well. In this research project, we use an asymmetry index defined as follows:

$$AI = 1 - \frac{A_{\text{overlap}}}{A_{\text{larger shape's area}}} \quad (4.7)$$

where  $A_{\text{overlap}}$  denotes the overlap area between two halves of the lesion and  $A_{\text{larger shape's area}}$  denotes the area of the larger shape.  $\frac{A_{\text{overlap}}}{A_{\text{larger shape's area}}}$  will output a symmetric index ranging from 0 (fully not symmetric) to 1 (fully symmetric). Then, we sub-

tract  $\frac{A_{overlap}}{A_{\text{larger shape's area}}}$  by 1 because we want the asymmetric index instead of the symmetric index. A perfect circle would output an asymmetry value of 0 because  $\frac{A_{overlap}}{A_{\text{larger shape's area}}}$  would equal 1 since all pixels are overlapping. We compute the asymmetric index both overlaps: and top/bottom (x-axis) and right/left (y-axis).

Finally, we compute the total asymmetric index by taking the mean asymmetric index for x-axis and y-axis. This is represented as follows:

$$AI_{total} = \frac{AI_x + AI_y}{2} \quad (4.8)$$

where  $AI_x$  and  $AI_y$  represent their asymmetric index for the x-axis and y-axis of the image.

In 4.5.1, we can see two examples of asymmetry index being applied to compare the left and right regions of the shape.

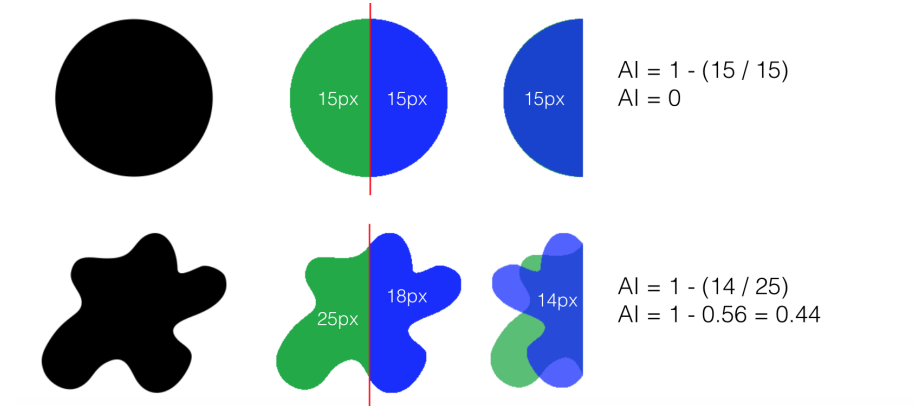


Figure 4.11: Examples of asymmetry index

#### 4.5.2 Border Irregularity

The second feature and one that is very important is the border irregularity of skin lesions. As expressed in 1.3, the edges and borders of malignant melanoma skin lesions are uneven and ragged. There are several ways to quantify this property.

#### Compactness Index

Compactness Index (CI), also known as Density Index, is the most popular measurement of a 2D object which measures the compactness an object. Retrieved from this paper

[26], compactness index is given by:

$$CI = \frac{P_L^2}{4\pi A_L} \quad (4.9)$$

where  $P_L$  is the perimeter of the lesion, and  $A_L$  is the area of the lesion. As a reminder, perimeter is defined as the distance around a two-dimensional shape and area is defined as the amount of space inside the boundary of a two-dimensional object.

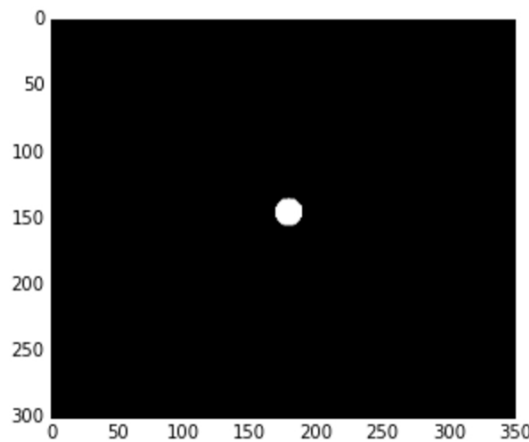


Figure 4.12: Example of an image of low edge abruptness

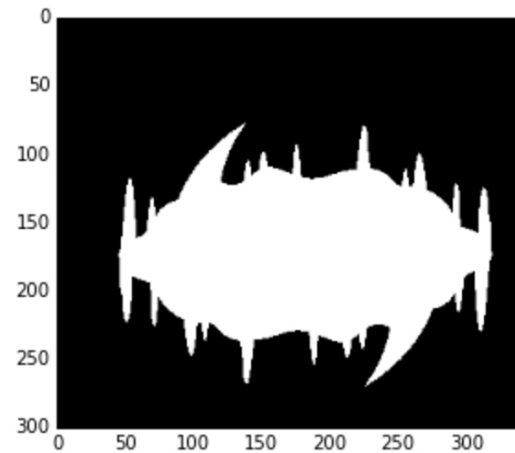


Figure 4.13: Example of an image of high edge abruptness

In the case of a perfect circle as demonstrated in Figure 4.12, CI would equal to 1 (represented in the equation below):

$$CI = \frac{P_L^2}{4\pi A_L} = \frac{(2\pi r)^2}{4\pi(\pi r^2)} = \frac{4\pi r^2}{4\pi r^2} = 1$$

Moreover, while the more irregular the shape is, the higher the CI would be. For the example in Figure 4.13, we compute that the area is 28,949 and the perimeter is 1,703. Putting it into the formula for Compactness Index, gives us an output of 7.98. This is due to it's large perimeter in comparison to it's relatively lower area.

However, this measure is very sensitive to noise along the border. Due to this, we need to include another measure for border irregularity.

### Edge Abruptness

Since we know that malignant melanoma skin lesions have rough edges, we need to find a way to measure the roughness. The intuition of the edge abruptness equation is to find the variance of radial distances from the centroid to the boundaries. As proposed by Guthowicz and Krustin [4], we can measure this by:

$$EA = \frac{\frac{1}{P_L} \sum_{p \subseteq C} (d(C, p) - \bar{m}_d)^2}{\bar{m}_d^2} \quad (4.10)$$

where EA denotes edge abruptness,  $P_L$  denotes the perimeter of the lesion,  $\bar{m}_d$  denotes the mean distance between the centroid and boundaries,  $d(C,p)$  denotes the distance between the centroid and boundary points, for each point in the set of boundary points. Intuitively, we divide all the variances by the perimeter because the perimeter is the number of pixels in the boundary. Hence, it would give an average of variances. Our results should show that benign skin lesions have low edge abruptness while malignant melanoma skin lesions have a high edge abruptness.

We can demonstrate further using two examples. Firstly, in the case of Figure 4.12 (perfect circle), EA would be 0 because there wont be any variance between the centroid to the boundary points. On the other hand, in the case of Figure 4.13 (ragged shape), we can see that the distance between the centroid and the boundary points are very inconsistent; hence causing a large variance and finally a large EA.

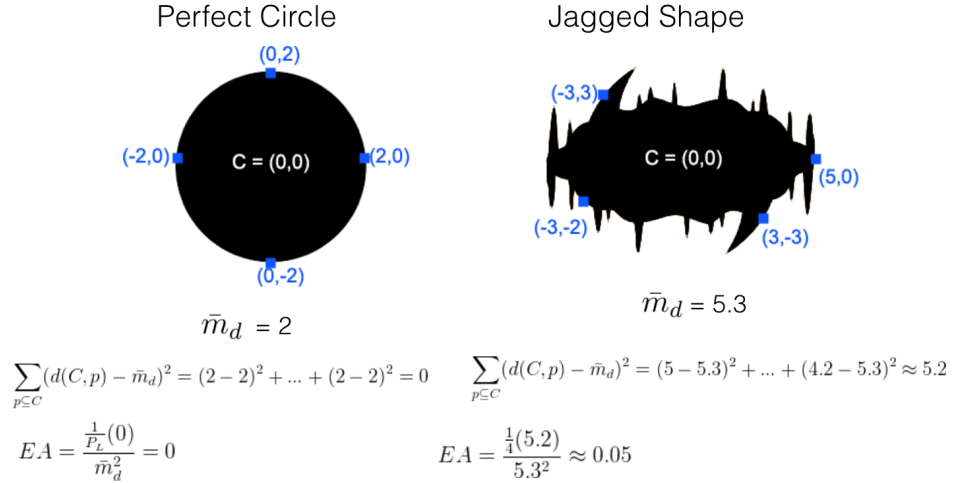


Figure 4.14: Examples of edge abruptness equation

#### 4.5.3 Color

Melanoma skin lesions tend to have different shades of color. So the first thing we did was try to quantify the colors of a skin lesion. I used a technique called K-Means clustering. The idea is to use K-Means clustering to determine the clusters of RGB values (in a 3-D space).

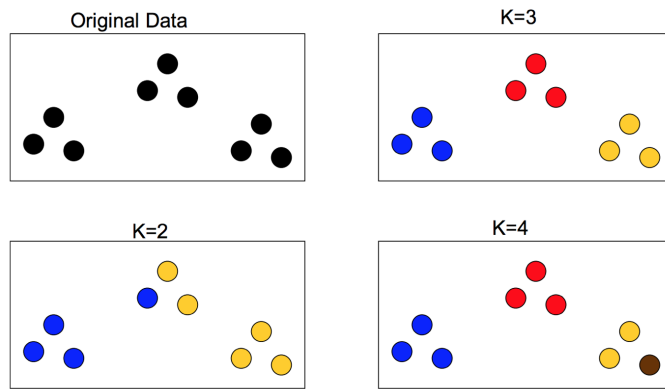


Figure 4.15: Example of clustering

Before we explain the K-Means part, I will first summarize the concept of clustering. Simple put, clustering is the process of finding groups in a set of data. By using clustering algorithms, we can find pattern of groups which share great similarity. As demonstrated in Figure 4.15, we can find K clusters in the sample dataset, where K

represents the number of clusters. K-Means clustering is an algorithm used to calculate clusters based on determining centroids of clusters using similarity algorithms. There are many ways of measuring distances between data points, the most common one and one which this paper uses is Euclidean distance, defined as follows:

$$d_{euclid}(x, y) = \sqrt{\sum_{i=1}^N (x_i - y_i)^2} = \sqrt{(x_1 - y_1)^2 + (x_2 - y_2)^2 + \dots + (x_N - y_N)^2} \quad (4.11)$$

where  $x_1$  to  $x_N$  are parameters for the x point and  $y_1$  to  $y_N$  are the parameters for the y point. For a 2-D space, the euclidean distance would be represented as

$$d_{euclid}(x, y) = \sqrt{(x_1 - y_1)^2 + (x_2 - y_2)^2}. \quad (4.12)$$

The K-Means cluster algorithm runs as follows:

1. Select k random data points as initial centroids
2. Repeat
  - (a) Assign each point to their nearest centroid using Euclidean distances.
  - (b) Recalculate the centroid of new clusters by taking the mean
3. Repeat until the centroids dont change

[33]

However, after implementing this algorithm, I have seen several cases of misinterpretation of colors due to the unnormalized color conditions. For example, Figure 4.16 shows an image with a high lighting conditions which affect the color of the skin lesion. Applying K-Means clustering to determine the top 3 color clusters, we get the colors represented in Figure 4.17 where we can see that the purple color appears due to

light reflection. Whereas if the lighting condition isn't as bright, the top 3 colors will probably be variations of brown color.



Figure 4.16: Image with high lighting conditions

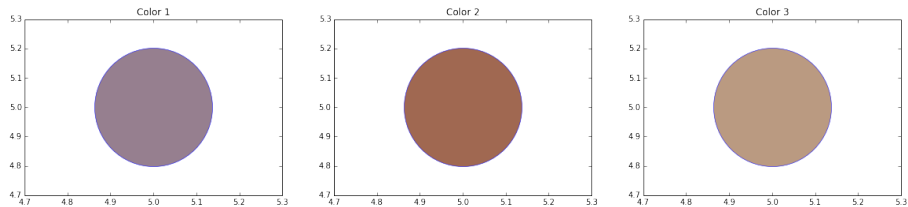


Figure 4.17: Color extraction phase of Figure 4.16

Due to these reasons, I didn't use K-Means clustering to extract color features. Instead we used two color features derived from this article [40] which are described below.

### Color Variation

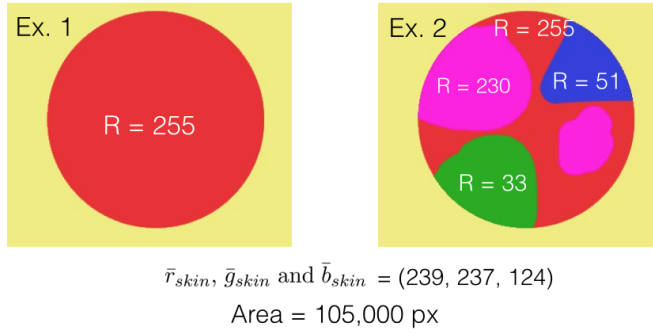
Since we know that the variance of colors in a lesion is an indicator for melanoma, we must study this. However, since we're aware that each image has different lighting conditions, we must compare the variation of colors relative to the skin's colors. The color variation metric is defined as follows [26]:

$$Var_{red} = \frac{\sum_{(x,y) \subseteq L} (r_{(x,y)} - \bar{r}_{skin})^2}{A_t} \quad (4.13)$$

$$Var_{green} = \frac{\sum_{(x,y) \subseteq L} (g_{(x,y)} - \bar{g}_{skin})^2}{A_t} \quad (4.14)$$

$$Var_{blue} = \frac{\sum_{(x,y) \subseteq L} (b_{(x,y)} - \bar{b}_{skin})^2}{A_t} \quad (4.15)$$

where  $r_{(x,y)}$ ,  $g_{(x,y)}$  and  $b_{(x,y)}$  represents the r, g and b values for the lesion. Moreover,  $A_t$  represents the total area of the lesion,  $\bar{r}_{skin}$ ,  $\bar{g}_{skin}$  and  $\bar{b}_{skin}$  represents the mean red, green and blue values for the skin part of the image [40]. This equation can be further visualized with the examples represented in figure 4.18.



$$\text{Ex. 1 } Var_{red} = \frac{(255 - 239)^2 + \dots + (255 - 239)^2}{105000} = 256$$

$$\text{Ex. 2 } Var_{red} = \frac{(255 - 239)^2 + \dots + (255 - 239)^2 + \text{Do same for pink} + \text{Do same for blue} + \text{Do same for pink}}{105000} \approx 7930$$

Figure 4.18: Two examples of color variation for red value

### Relative Chromaticity of RGB Values

Since we now know that the lighting condition affects the color extraction of an image, we need to study the colors of each image independently. Relative chromaticity is the measure of an objects colors independent of the luminance. It is represented using the following formula derived from [26]:

$$RC_{red} = \frac{\bar{r}_{lesion}}{\bar{r}_{lesion} + \bar{g}_{lesion} + \bar{b}_{lesion}} - \frac{\bar{r}_{skin}}{\bar{r}_{skin} + \bar{g}_{skin} + \bar{b}_{skin}} \quad (4.16)$$

$$RC_{green} = \frac{\bar{g}_{lesion}}{\bar{r}_{lesion} + \bar{g}_{lesion} + \bar{b}_{lesion}} - \frac{\bar{g}_{skin}}{\bar{r}_{skin} + \bar{g}_{skin} + \bar{b}_{skin}} \quad (4.17)$$

$$RC_{blue} = \frac{\bar{b}_{lesion}}{\bar{r}_{lesion} + \bar{g}_{lesion} + \bar{b}_{lesion}} - \frac{\bar{b}_{skin}}{\bar{r}_{skin} + \bar{g}_{skin} + \bar{b}_{skin}} \quad (4.18)$$

where  $\bar{r}_{lesion}$ ,  $\bar{g}_{lesion}$  and  $\bar{b}_{lesion}$  represent the average red, green and blue of the lesion area and  $\bar{r}_{skin}$ ,  $\bar{g}_{skin}$  and  $\bar{b}_{skin}$  represent the average red, green and blue values of

the skin area. By dividing the colors mean with the sum of all the colors means, we find out how strong that particular color is (do this for both skin and lesion). For example, if the  $\bar{r}_{lesion} = 100$ ,  $\bar{g}_{lesion} = 100$  and  $\bar{b}_{lesion} = 100$ , we can see that it would output  $\frac{\bar{r}_{lesion}}{\bar{r}_{lesion} + \bar{g}_{lesion} + \bar{b}_{lesion}} = \frac{100}{300}$  for the red value of the lesion. However, if  $\bar{r}_{lesion} = 200$ , it would output  $\frac{200}{400}$  for red,  $\frac{100}{400}$  for green and  $\frac{100}{400}$  for blue in the lesion. This fraction shows the strength of the particular color as compared to their own section (skin or lesion). We do this for both the skin and the lesion.

Moreover, we subtract the lesions strength with the skins strength for each red, green and blue value. Hence, this outputs the value of the strength of each color in the lesion independent of the skin [40]. Relative chromaticity can be further visualized using the examples in Figure 4.19.

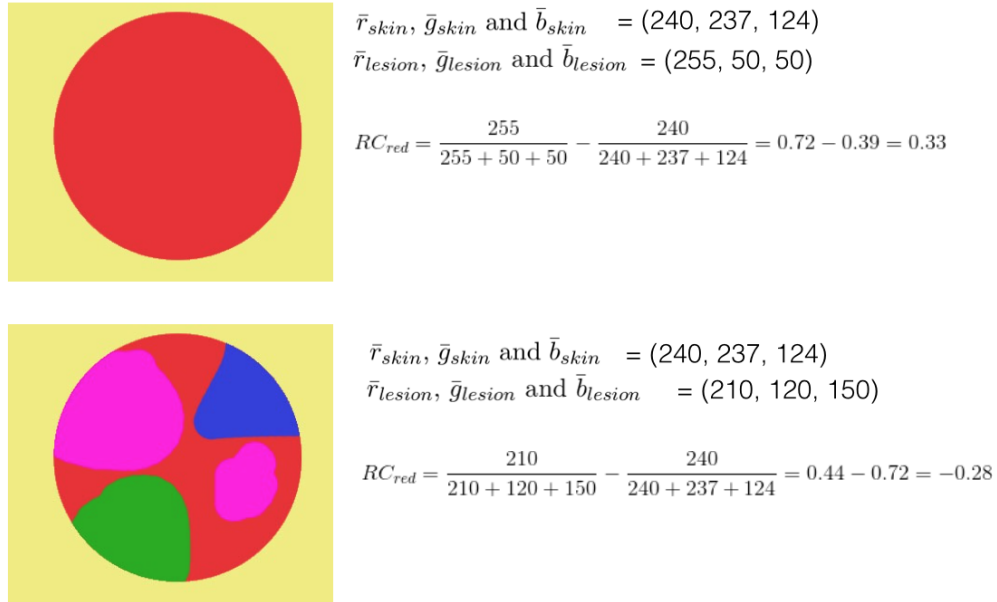


Figure 4.19: Two examples of relative chromaticity for red value

#### 4.5.4 Diameter

As we reviewed in Section 1.3, diameter is a crucial factor in determining whether or not a skin lesion is benign or cancerous. As a rule of thumb, Melanoma skin lesions

tend to have a diameter of 4mm or greater. This makes it easy to diagnose while using a measuring tape or ruler. However, since my research project is a computer-based diagnosis, we cannot use measuring tapes or rules. If we were simply to compute the diameter of the lesion, this number wont suffice. This is because different images are zoomed in differently. For example, Figure 4.20 shows a highly zoomed image while Figure 4.21 shows a relatively zoomed out image. Due to this inconsistency in zoom distances of images, I decided to remove this section from my model.



Figure 4.20: Image with high zoom



Figure 4.21: Image with low zoom

#### 4.5.5 Evolution

A lesion that evolves in shape, diameter, color or border irregularity is a main indication of a malignant skin lesion. We can track the evolution of a skin lesion by simply comparing the measurements over a period of time based on the aforementioned algorithms and equations. Since this paper is based on a research project instead of an application/software, I decided to leave this section out.

## 4.6 Classification Model

Machine learning is a branch of computer science that explores how to automatically learn and detect patterns in data to make accurate predictions. A model is built from past observations (training data) in order to make data-driven predictions with new data (test data). The training and test data is derived from the feature extraction stage.

Machine learning is typically divided into three areas [29]:

1. Supervised Learning - analyzes the labeled training data in order to make predictions with test data. A popular example is trying to categorize whether an email is spam or not spam. We can train an existing dataset of emails to make predictions for future emails.
2. Unsupervised Learning - analyzes unlabeled training data in order to identify patterns or hidden structures in the data. For example, if we were assigned to build three pizza delivery centers based on their 30 customer locations, we would utilize clustering to try and pick the best locations to open the three delivery centers. Our model would label the 30 customer locations based on the closest delivery center.
3. Reinforcement Learning - a program which interacts with its environment where it must perform a certain goal without being explicitly told. It achieves the goal by receiving rewards/reinforcements from its environment. For example, reinforcement learning is used in game playing to predict the next best move without explicitly being told.

In this research paper, I have evaluated three variations of Support Vector Machines: linear SVM, radial SVM and quadratic SVM. For all three models, we use the five features described in Section 4.5 as the input. Those are asymmetry index, compactness index, edge abruptness, color variation, relative chromaticity. Moreover, the image data set is separated into training data, which consists of 60% of the images (40 images) and the test data, which consists of 40% of the images (27 images).

Support Vector Machine is a popular type of supervised learning where the goal is to correctly identify which class a data belongs to using a classifier. By creating a classifier with a training set of data and their correctly identified classes, we can predict new observations using this classifier. For a feature vector of two dimensions, a classifier is a single line which separates the two classes of data. Whereas in a 3-D plot, the classifier is represented as a plane.

SVM has many benefits and is arguably one of the best classification algorithms currently existing. One of the benefits is that the SVM maximizes the margin between the hyperplane and the support vectors. Support vectors are defined as the data points of both classes which are closest to the hyperplane (circled in Figure 4.6). For example in Figure 4.6,  $x$  classifier is chosen by the SVM because it correctly separates the two classes of data and creates the largest possible margin between the hyperplane and the support vectors. This is an example of a linear form of SVM.

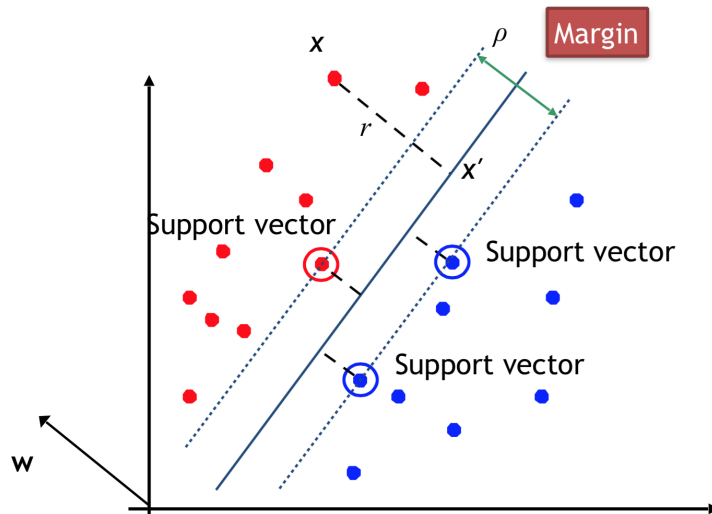


Figure 4.22: Support Vector Machine

#### 4.6.1 Linear SVM

Linear SVM's are the most basic form as demonstrated above. It is simply used when a dataset can be divided by a linear classifier. No mapping to a higher dimension needs to

be done as it's already separable.

The general form of an linear SVM decision boundary is defined as below:

$$f(x) = w_1 \cdot x + w_0 \quad (4.19)$$

Where:

$$f(x) = \left( \sum_{i=1}^N a_i y_i x_i \right)^T x + w_0 \quad (4.20)$$

where  $a_i = 0$  for all but few points (support vectors),  $y$  is the class -1 or 1 for the corresponding data point  $x_i$  and  $N$  is the number of data points.

In addition, SVM also deals well with nonlinear data classifications. SVM utilizes a technique called kernel trick where we map a dataset into a higher dimension in order to find for it to be classifiable. It is called kernel trick because the mapping does not need to be every computed. Since our algorithm is expressed using a dot product, we simply need to replace the dot product with a kernel function. There are many types of kernel functions available. This paper covers three types of kernels: linear (discussed above), radial and quadratic kernels.

#### 4.6.2 Radial Kernel

Radial kernels are used to transform data into a radial shaped data space and is the most popular kernel. For example, since the left of Figure 4.6.2 isn't linearly separable, we can transform it into a higher dimension (3-D) where a 2-D plane can separate the data. We use a radial basis function (RBF) in order to transform this data into a higher dimension. The RBF is defined as:

$$k(x, x') = \frac{(-\|x - x'\|)^2}{2\sigma^2} \quad (4.21)$$

which when substituted into  $f_{rbf}(x) = \sum_i^N a_i y_i k(x, x_i)$  equation becomes:

$$f_{rbf}(x) = \sum_i^N a_i y_i \exp\left(\frac{-\|x - x_i\|^2}{2\sigma^2}\right) + b \quad (4.22)$$

where  $\sigma$  is a free parameter used as the strength for each point. The sigma must be tuned accordingly. If the sigma is too high, it will behave almost linearly. However,

if this sigma is too low, the decision boundary will be highly sensitive to noise in the training data. Please note that the RBF kernel will output a range of 0 to 1.

[1]

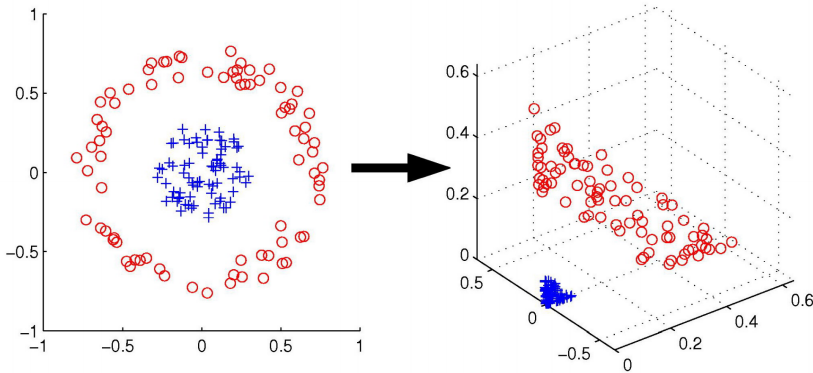


Figure 4.23: RBF Kernel Trick

#### 4.6.3 Quadratic Kernel

Similar to radial kernels, polynomial kernels also map the dataset into a higher dimension.

Polynomial kernels are defined by:

$$k(x, y) = (x^T y + c)^2 \quad (4.23)$$

where  $x$  and  $y$  are vectors of the input space,  $c$  is non-negative free parameter.

For example, if we choose that we are going to map to a polynomial kernel defined by:

$$k(x, y) = (x * y)^2 = x_1^2 y_1^2 + 2u_1 v_1 u_2 v_2 + u_2^2 v_2^2, \quad (4.24)$$

we can see that our data will now be 3 dimensional.

## CHAPTER 5

### EXPERIMENTAL RESULTS

#### 5.1 Preprocessing Results

As discussed in Section 4.3, this paper used three image preprocessing techniques to prepare for the segmentation phase. RGB to grayscale, size normalization and denoising (using median filtering) was used.

	Success Rate	
	MACWE	Otsus Method
Grayscale + Size Normalization	27 (pos) + 20 (neg) $= 47/109 = 46.6\%$	20 (pos) + 11 (neg) $= 33/109 = 30.3\%$
Grayscale + Size Normalization + Median Filter	46 (pos) + 22 (neg) $= 68/109 = 62.4\%$	33 (pos) + 16 (neg) $= 49/109 = 44.9\%$

Table 5.1: Impact of preprocessing images

In Table 5.1, I examine the effectiveness of the preprocessing methods by comparing it with the image segmentation results. As we can see from the results, preprocessing the images plays a crucial role to segment a skin lesion. We can see that while preprocessing the image with grayscale and size, the results of image segmentation are 46.6% for MACWE and 30.3% for Otsus method. However, when incorporating median filtering for denoising, the successfully segmented images reach 62.4% and 44.9% respectively. Please note that these results/success rate are defined by the number of successfully segmented lesions divided by the total number of lesions. An example of a successfully segmented lesion versus a poorly segmented lesion can be found in Figure 5.1.

#### 5.2 Image Segmentation Results

Incorporating the preprocessing techniques discussed, I then studied the segmentation results and tried to derive an explanation for success or failure of particular images. Below

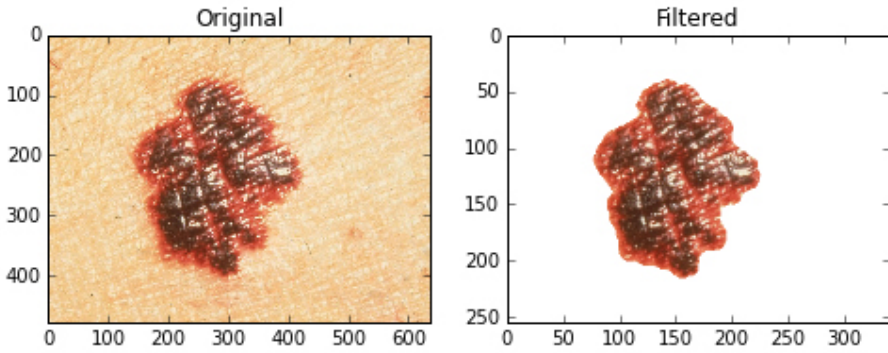


Figure 5.1: Comparison of a well segmented lesion (left) with a poorly segmented lesion (right)

is a breakdown of images and their success rates with both algorithms. As identified in the above section, the results/success rate are defined by the number of successfully segmented lesions divided by the total number of lesions.

	No. of Images	MACWE (correctly segmented images)	MACWE (success rate)	Otsus Method (correctly segmented images)	Otsus Method (success rate)
Melanoma Images	74	46	62.1%	33	44.6%
Benign Images	35	22	62.9%	16	45.7%
Total	109	68	62.4%	49	44.9%

Table 5.2: Comparison of MACWE and Otsus Method

From the results in Table 5.2, we can safely conclude that Morphological Active Contour Without Edges (MACWE) is the more successful image segmentation algorithm while compared to Otsus method. The success rate of both image classes for MACWE is 62.4% whereas Otsus method is 44.9%.

I observed that Otsus method doesn't work well with images with a lot of noise. There are several images containing elements other than the mole. For example, Figure 5.2 shows that Otsus method segmented the measuring tape from the image. In contrary, we see that MACWE can successfully segment the mole from the same image.

### 5.3 Statistical Summary of Feature Extraction

In Table 5.3, the statistical summary of the features from the feature extraction stage is provided. We can examine the success/failure from the feature extraction phase by

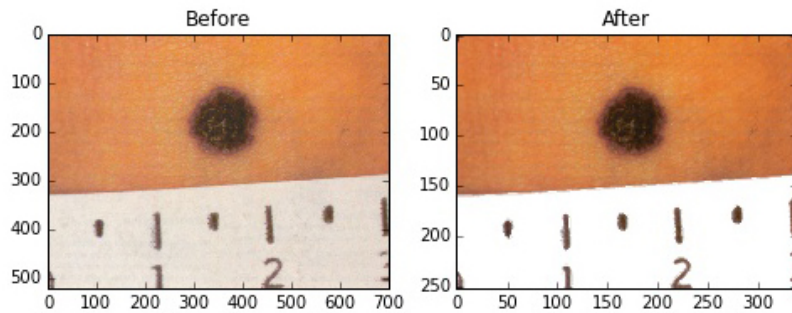


Figure 5.2: How MACWE and Otsu's Method deals with large noise

	Mean		Standard Deviation	
	Melanoma Lesions	Benign Lesions	Melanoma Lesions	Benign Lesions
Asymmetry Index	0.440	0.426	0.256	0.434
Compactness Index	1.728	1.326	0.425	0.208
Edge Abruptness	0.064	0.105	0.180	0.317
Color Variation (Red)	19359.835	22319.996	10022.295	13588.790
Color Variation (Green)	33290.875	35278.107	5968.918	9757.180
Color Variation (Blue)	37556.587	40269.987	6176.257	8807.688
Relative Chromaticity of RGB Values (Red)	0.121	0.112	0.0730	0.080
Relative Chromaticity of RGB Values (Green)	-0.041	-0.034	0.026	0.028
Relative Chromaticity of RGB Values (Blue)	-0.079	-0.078	0.053	0.055

Table 5.3: Statistics of features extracted

comparing it to our knowledge of the ABCDE properties of melanoma.

- Asymmetry Index: The mean asymmetry index of both melanoma and benign lesions are very similar (0.440 and 0.426). This shows that this feature was not properly extracted. One reason could be due to the photos being taken from different angles affecting the symmetric property.
- Compactness Index: The mean compactness index of the two classes are spread out (1.748 for melanoma and 1.326 for benign) and are in accord to our knowledge of how benign lesions have smoother boundaries. Remember: The lower the compactness index, the more round and smooth the lesion is. Moreover, the standard

deviations are relatively narrow. These reasons show that compactness index is a successful feature metric.

- Edge Abruptness: The mean edge abruptness of the two classes are quite similar (approximately 0.05 difference) and standard deviation is very wide. This shows that edge abruptness was not a successful metric.
- Color Variation (RGB): The color variation of the RGB values are moderately spread out (approximately 3000 difference for red, 2000 difference for green and 3000 difference for blue). However, the standard deviation is very wide. Hence, we cannot conclude whether this feature was successful or unsuccessful.
- Relative Chromaticity (RGB): The mean values of each RGB for benign and melanoma lesions are very similar. Moreover, the standard deviation is wide. Hence, this feature was unsuccessful.

#### 5.4 Scatterplot Summary of Feature Extraction

In addition to the statistical summary of feature extraction, a scatterplot summary can be used identify the effectiveness and relationship between the features with respect to the classes. This scatterplot compares each feature with each other and plots the points. For example, if we are to study the feature extraction of Asymmetry Index and Compactness Index, we would first create a scatter plot of Asymmetry Index (x - axis) and Compactness Index (y - axis). We must separate the points of the scatterplot into two different labels; for Melanoma and benign cases. From here, we can study the relationship where the sparseness between the two classes represent a successful feature extraction for the two features. Moreover, if the benign and Melanoma points are mostly overlapped, this shows that these two features are relatively unsuccessful.

In our case we have 9 features: Color Homogeneity Variance(R), Color Homogeneity Variance(G), Color Homogeneity Variance(B), Color Relative Chromaticity(R), Color Relative Chromaticity(G), Color Relative Chromaticity(B), Asymmetry, Compact-

ness Index and Edge Abruptness. Hence, we have a 9 x 9 scatterplot. The diagonal of this scatterplot are histogram plots representing the number of occurrences of numbers in that particular feature. The table below shows the scatterplot summary for this project's feature extraction. Please note that the Melanoma points are denoted as 'x' in red color and benign points are denoted as 'o' in blue color. This table is divided into two subsections (due to the large size) which can be found in Figure 5.3 and 5.4.

From the table, we can draw some conclusions about our success/failure in the feature extraction phase as follows:

- Asymmetry Index: While compared to other features, we can see that the asymmetry index is not very successful in separating melanoma with benign cases. Since most of the points overlap while comparing asymmetry with other features, this shows that asymmetry index isn't a successful feature.
- Compactness Index: While comparing compactness index to other features, we see that the data points between melanoma and benign cases are very spread out and distinguished. This confirms that compactness index is a successful feature.
- Edge Abruptness: It is clear that this feature is not a successful one because nearly all the points of each plot comparison are overlapped. This is a surprising outcome which leads me to believe that there was a problem extracting this data.
- Color Variation (combined RGB): While comparing color variation to other features, we can see that color variation is not a very successful feature because the melanoma and benign data points are very overlapped.
- Relative Chromaticity (combined RGB): From the rows of Relative Chromaticity (R, G, B), we can see that most of the data points of melanoma and benign are overlapping. This shows that this feature wasn't successful. Color variation and relative chromaticity has given me doubts in the implementation stage and the scatterplot analysis confirms that. We must look at other alternatives to extract

color features from images.

## 5.5 Classification Results

After the feature extraction process is completed, I then evaluated several classification models and compared their results. From the 68 correctly segmented images, I separated it into training data, which consists of 60% of the images (40 images) and test data, which consists of 40% of the images (28 images). Then, I analyzed the results of the classifiers based on random assignments of training and test data which is fed into each model. This is repeated 10,000 times for each model.

	Accuracy Rate (Mean of 10,000 repetitions)	Standard Deviation (10,000 repetitions)
SVM (linear)	71.5%	7.57%
SVM (radial)	69.4%	8.07%
SVm (quadratic)	70.1%	7.41%

Table 5.4: Comparison of algorithms' accuracy rates at default threshold of 0.5

As we can see in Table 5.4, the linear SVM is the most successful model acquiring 71.5% accuracy in detecting melanoma and benign cases. Coming in at a close second is the quadratic SVM which has accuracy of 70.1%. It may be suspicious that the quadratic SVM's accuracy rate is poorer than the linear SVM's accuracy rates. I suspect that there may be overfitting in the model. Please note that this accuracy rate is when the threshold is at 0.5. However, this is not enough to determine the success/failure of the algorithm. We need to study the performance when varying the threshold. This is done using ROC Analysis.

## ROC Analysis

Receiver Operator Characteristics (ROC) is a metric used to evaluate the predictive behavior of a classifier. Using confusion matrices for each model, we can visualize the performance of the classifier. A confusion matrix consists of the following equations

and terminology as described below [25]:

- Positive (P) = No. of Melanoma cases
- True Positive (TP) = No. of correctly identified Melanoma cases
- True Negative (TN) = No. of correctly identified benign cases
- Negative (N) = No. of benign cases
- False Positive (FP) = No. of cases where the algorithm diagnosed as Melanoma, but it is benign
- False Negative (FN) = No. of cases where the algorithm diagnosed as benign, but it is Melanoma

Note: The TP, FP, TN and FN figures are computed by averaging the 10,000 iterations' results. Then I computed a confusion matrix for each of the three variations of SVM to understand the model better. Please note, however, that these numbers are at a default threshold of 0.5 so we must be aware that the numbers represented in the confusion matrices are subject to change with different thresholds.

	True Diagnosis	
Predicted Diagnosis	Positive (Melanoma)	Negative (Benign)
Positive (Melanoma)	TP = 15.57	FP = 4.63
Negative (Benign)	FN = 3.34	TN = 4.46

Table 5.5: Confusion matrix for Support Vector Machine (Linear)

For medical diagnosis like this research projects algorithm, false negative cases are the most crucial ones. As a reminder, false negative diagnosis is when the algorithm states that the results are false (not cancerous), when in reality they are positive (cancerous). This is the most crucial because, if employed in medical practice, if a patient

		<b>True Diagnosis</b>	
<b>Predicted Diagnosis</b>		Positive (Melanoma)	Negative (Benign)
Positive (Melanoma)		TP = 17.12	FP = 6.77
Negative (Benign)		FN = 1.79	TN = 2.32

Table 5.6: Confusion matrix for Suppor Vector Machine (Radial)

		<b>True Diagnosis</b>	
<b>Predicted Diagnosis</b>		Positive (Melanoma)	Negative (Benign)
Positive (Melanoma)		TP = 18.55	FP = 8.02
Negative (Benign)		FN = 0.35	TN = 1.07

Table 5.7: Confusion matrix for Suppor Vector Machine (Quadratic)

is victim to a false negative case, he/she will not know she has melanoma. This has huge consequences and can eventually lead to a loss of life. On the other hand, false positive cases are ones that the result shows positive (cancerous), when in reality it is false (not cancerous). Even though we want to reduce false positive cases as much as possible, medical professionals can still conduct more tests in order to determine the true diagnosis. We can determine false negative rate and false positive rate by:

$$\text{False Negative Rate (FNR)} = \frac{FN}{P} = \frac{FN}{FN + TP} \quad (5.1)$$

$$\text{False Positive Rate (FPR)} = \frac{FP}{P} = \frac{FP}{FP + TN} \quad (5.2)$$

Moreover, we can use the true positive rate and true negative rate to determine the number of cases where the model identifies correctly that a case is positive (cancerous) and negative (not cancerous), respectively:

$$\text{True Positive Rate (TPR)} = \frac{TP}{P} = \frac{TP}{TP + FN} \quad (5.3)$$

$$\text{True Negative Rate (TNR)} = \frac{TN}{N} = \frac{TN}{TN + FP} \quad (5.4)$$

As identified in Table 5.8, the linear and quadratic SVM deem most successful (at threshold = 0.5). The linear SVM succeeds in achieving the least false positive rate

	False Positive Rate (FPR)	False Negative Rate (FNR)	True Positive Rate (TPR)	True Negative Rate (TNR)
SVM (linear)	0.509	0.176	0.824	0.491
SVM (radial)	0.744	0.095	0.905	0.256
SVM (quadratic)	0.882	0.019	0.981	0.118

Table 5.8: ROC Analysis Summary at threshold = 0.5

and the best true negative rate. Whereas the quadratic SVM achieves the lowest false negative rate and highest true positive rate. It may be difficult in picking the best model to use because they are drawbacks to each one. If we pick the quadratic model, we will achieve the least false negative rate (meaning that only 1.9% of the peoples cases would be diagnosed benign while in fact they are malignant). However, we also notice that the false positive rate of this model is very high at 88.2%. We can discover that this means that the quadratic model nearly always gives a positive output. Moving on to the linear SVM, it has a false positive rate of 50.9% (which is the least compared to the other models), however, has a false negative rate of 17.6% which is the highest compared to other models. Hence, we can see that they are tradeoffs between models and no best model can be picked as of yet.

However, these rates are only at a threshold of 0.5. Our next goal is to discover these rates at different, varying thresholds. To do this, we will need to draw an ROC curve. To draw an ROC curve, only the TPR (y-axis) and FPR (x-axis) are needed. The FPR and TPR are plotted at various threshold settings from 0 to 1. We can use the ROC curve study the performance of each model by calculating the area under the curve. The model with the best performance would have the least FPR and the most TPR, where the AUC would be 1. As we can see from our ROC curve in Figure 5.5, our Linear SVM model is more successful because it generates the highest area under the curve at 0.79, while Radial SVM comes in second at 0.7. Moreover, we can analyze the performance of certain thresholds and compare the results. For example, at  $FPR = 0.4$ , we can see that the Linear SVM generates a FPR of approximately 0.81, while the Radial SVMs FPR is

approximately 0.65 and lastly, the Quadratic SVM is approximately 0.1.

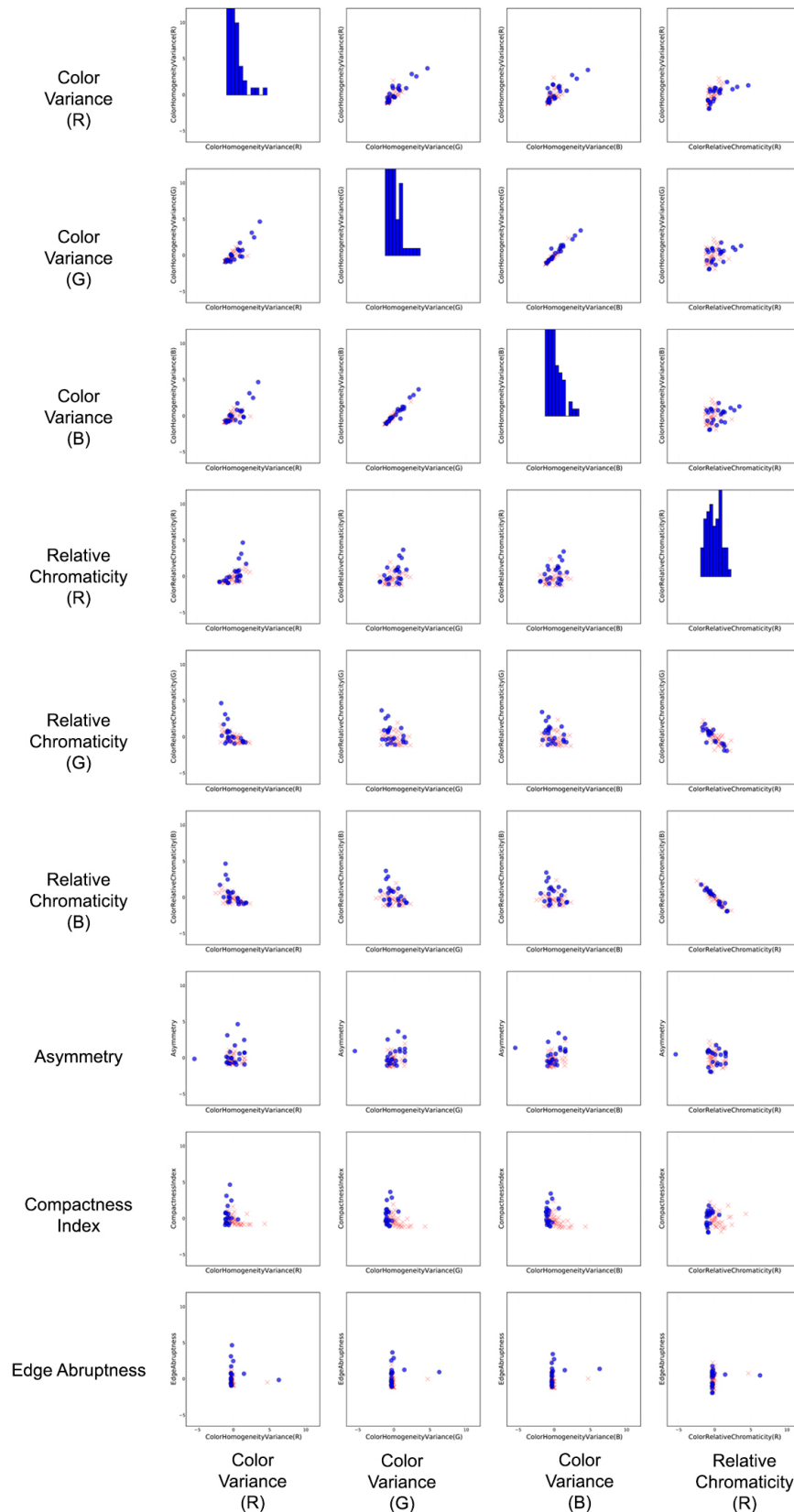


Figure 5.3: Scatterplot summary of feature extraction (part 1)

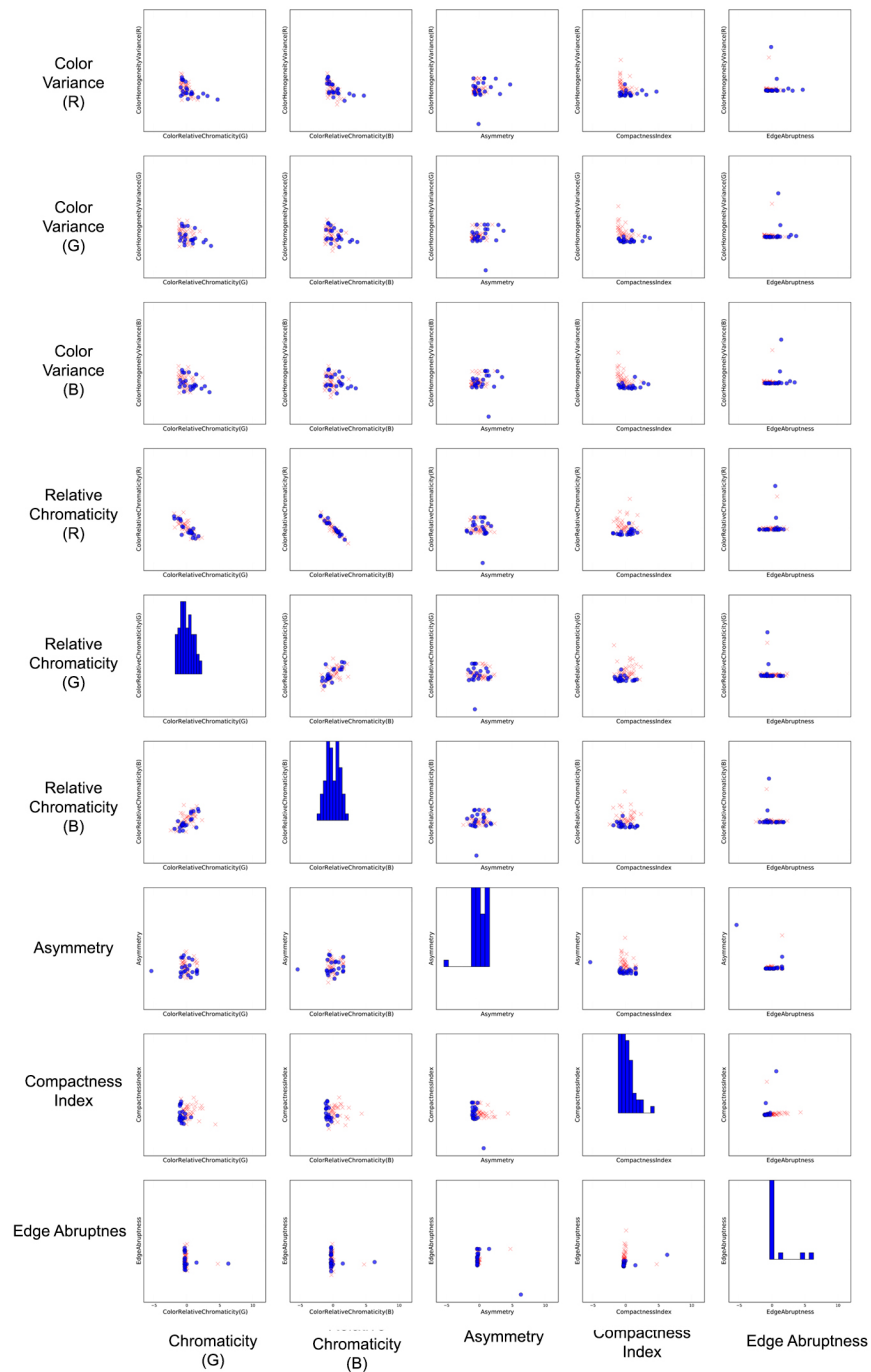


Figure 5.4: Scatterplot summary of feature extraction (part 2)

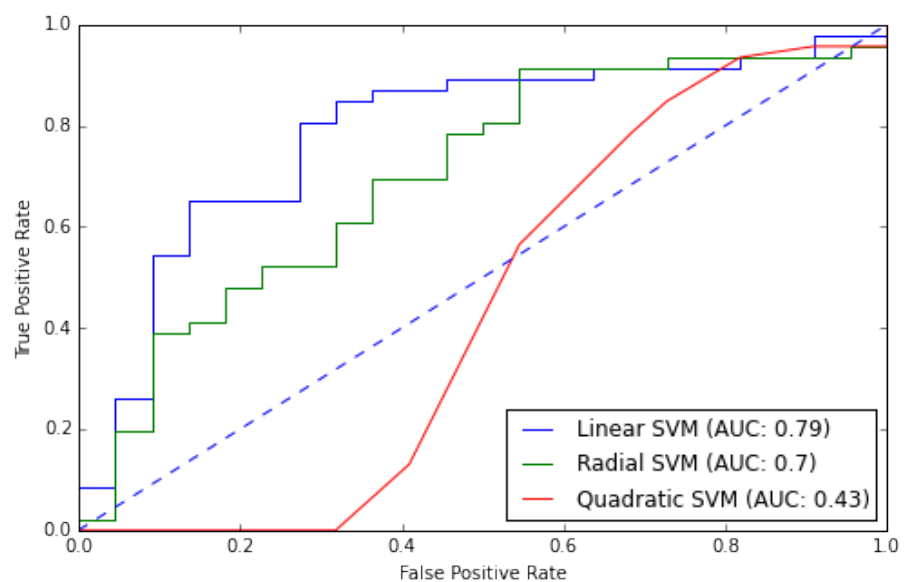


Figure 5.5: Comparison of algorithms using ROC Curve

## CHAPTER 6

### CONCLUSION

In conclusion, this research paper aims to provide a foundation of how feature extraction methods and machine learning algorithms can be utilized to detect melanoma from skin lesion images. This research paper discusses two images segmentation methods (Otsus method and MACWE) used to segment the lesion from the image. Next, five features are being extracted from the segmented lesion: asymmetry index, compactness index, edge abruptness, color variation and relative chromaticity of RGB values. Finally, after extracting the five features from Melanoma images, this research paper experiments with three forms of support vector machine algorithms; linear, radial and quadratic. As discussed in Chapter 5, the linear and quadratic SVM models prove to be the better ones, however, both have tradeoffs. We then analyzed the models using an ROC curve which allowed us to visualize the models' performances at different thresholds.

#### 6.1 Future Work

This research project needs to be further researched and developed in order to improve its success/failure rate. In order to make our model stronger, I believe we need a larger dataset of images with controlled environment, possibly from a hospital or skin clinic. With a controlled environment, it would be much easier for the image segmentation process and the feature extraction process is less prone to errors. Moreover, as identified from Chapter 5, only two of the features were meaningful. We need to include more meaningful features which play a larger role in determining melanoma from benign moles. Lastly, with a larger dataset, we can then again test the success/failure of a classification model.

## REFERENCES

- [1] Zisserman A. Svm dual, kernels and regression. "<http://www.robots.ox.ac.uk/~az/lectures/ml/lect3.pdf>", 2015.
- [2] Ce marking approval for medical devices in europe. "<http://medicaldevices.bsigroup.com/en-GB/our-services/ce-marking/>",.
- [3] Bailey Eileen. Misdiagnosis or brushing aside signs of skin cancer: The importance of seeing a specialist. "<http://www.healthcentral.com/skin-cancer/c/1443/158285/misdiagnosis/>", jan 2013.
- [4] Zagrouba Ezzeddine and Barhoumi Walid. A preliminary approach for the automated recognition of malignant melanoma. *Image Analysis & Stereology*, 2004.
- [5] Melanoma Research Foundation. Getnaked. it's pretty simple, really. "<http://www.melanoma.org/get-involved/advocacy-initiatives/get-naked>".
- [6] The Skin Cancer Foundation. Do you know your abcdes? "<http://www.skincancer.org/skin-cancer-information/melanoma/melanoma-warning-signs-and-images/do-you-know-your-abcdes>".
- [7] Wikimedia Foundation. Grayscale. "<https://en.wikipedia.org/wiki/Grayscale>".
- [8] Erdmann Friederike, Lortet-Tieulent Joannie, Schuz Joachim, Zeeb Hajo, Breitbart Rudiger, Greinert amd Eckhard, and Bray Freddie. International trends in the incidence of malignant melanoma 19532008 - are recent generations at higher or lower risk? *International Journal of Cancer*, 2013.
- [9] Sapiro Guillermo. Otsu's image segmentation algorithm. "[https://www.youtube.com/watch?v=b4Hg2t\\_tmn4](https://www.youtube.com/watch?v=b4Hg2t_tmn4)", mar 2013.
- [10] Singh Hardeep, Meyer Ashley, and Thomas Eric. The frequency of diagnostic errors in outpatient care: estimations from three large observational studies involving us adult populations. *BMJ Quality & Safety*, 2014.
- [11] "[http://www.medicinenet.com/skin\\_cancer\\_pictures\\_slideshow/article.htm](http://www.medicinenet.com/skin_cancer_pictures_slideshow/article.htm)".
- [12] "<http://www.dermatology.org/molemelanoma/watch2.html>".

- [13] "http://www.skinsight.com/teen/commonAcquiredNevusMole.htm".
- [14] "http://irishskinfoundation.ie/skin-conditions/melanoma-skin-cancer-gallery".
- [15] "http://www.your-doctor.net/dermatology\_atlas/english/?id=19".
- [16] "http://homepages.inf.ed.ac.uk/rbf/DERMOFIT/".
- [17] "https://www.skinvision.com/mole-images/normal".
- [18] "http://www.cancer.gov/types/skin/melanoma-photos".
- [19] "http://www.macmillan.org.uk/information-and-support/melanoma/diagnosing/how-cancers-are-diagnosed/signs-and-symptoms/signs-symptoms-melanoma.html#tcm:9-9907".
- [20] "https://en.wikipedia.org/wiki/Melanoma".
- [21] "http://scikit-image.org/docs/dev/user\_guide/tutorial\_segmentation.html".
- [22] "http://www.skincheck.org/Page4.php".
- [23] "https://visualsonline.cancer.gov/details.cfm?imageid=9784".
- [24] "http://hardinmd.lib.uiowa.edu/dermnet/melanoma5.html".
- [25] Holder Larry. Roc analysis for evaluation of machine learning algorithms. "http://www.eecs.wsu.edu/~holder/courses/cse6363/spr04/slides/ROC.pdf".
- [26] Bhuiyan Md.Amran, Azad Ibrahim, and Uddin Md.Kamal. Image processing for skin cancer features extraction. *International Journal of Scientific & Engineering Research*, 4, feb 2013.
- [27] Vala Miss Hetal J. and Baxi Prof. Astha. A review on otsu image segmentation algorithm. *International Journal of Advanced Research in Computer Engineering & Technology (IJARCET)*, 2(2), feb 2013.
- [28] Marquez-Neila Pablo, Baumela Luis, and Alvarez Luis. A morphological approach to curvature-based evolution of curves and surfaces. *IEEE TRANSACTIONS ON PATTERN ANALYSIS AND MACHINE INTELLIGENCE*, 2014.
- [29] Schapire Rob. Machine learning algorithms for classification. "http://www.cs.princeton.edu/~schapire/talks/picasso-minicourse.pdf".
- [30] Skinvision. "http://skinvision.com/", .

- [31] Skin cancer detection app skinvision now as accurate as a dermatologist. "<http://www.ibtimes.co.uk/skin-cancer-detection-app-skinvision-now-accurate-dermatologist-1501804>".
- [32] American Cancer Society. Melanoma skin cancer. "<http://www.cancer.org/acs/groups/cid/documents/webcontent/003120-pdf.pdf>".
- [33] Wittman Todd. Clustering. "<http://www.math.ucla.edu/~wittman/10c.1.11s/Lectures/Lec22.pdf>".
- [34] Tony, Luminita Chan, and Vese. An active contour model without edges.
- [35] Cancer Research UK. Skin cancer statistics. "<http://www.cancerresearchuk.org/health-professional/cancer-statistics/statistics-by-cancer-type/skin-cancer/incidence#heading-Six>".
- [36] ME Vestergaard, P Macaskil, PE Holt, and SW Menzies. Dermoscopy compared with naked eye examination for the diagnosis of primary melanoma: a meta-analysis of studies performed in a clinical setting. *National Center for Biotechnology Information*, 2008.
- [37] Ibm watson. "<http://www.ibm.com/smarterplanet/us/en/ibmwatson>".
- [38] Ibm research scientists investigate use of cognitive computing-based visual analytics for skin cancer image analysis. "<https://www-03.ibm.com/press/us/en/pressrelease/45710.wss>", dec 2014.
- [39] Ibm opens watson competency centre in victoria. "<http://www.zdnet.com/article/ibm-opens-watson-competency-centre-in-victoria/>", oct 2015.
- [40] Chang Ying, Stanley R. Joe, Moss Randy H., and Stoecker William Van. A systematic heuristic approach for feature selection for melanoma discrimination using clinical images. *National Institute of Health*, 2011.

## BIOGRAPHY

<b>NAME</b>	Patrachai Sachathamakul
<b>DATE OF BIRTH</b>	4th May 1993
<b>PLACE OF BIRTH</b>	Bangkok, Thailand
<b>INSTITUTIONS ATTENDED</b>	Ruamrudee International School, 2007-2011 Certificate of High School (Grade 12) Mahidol University, 2011-2015 Bachelor of Science (Computer Science)
<b>HOME ADDRESS</b>	25/16 Soi Charoenchai, Sukhumvit 63 Klong Toei, Bangkok 10110, Thailand
<b>E-MAIL</b>	sohum2002@hotmail.com